RESEARCH ARTICLE

Blow-Spun Si₃N₄-Incorporated Nanofibrous Dressing with Antibacterial, Anti-Inflammatory, and Angiogenic Activities for Chronic Wound Treatment

Pengchao Ma[1] · Chun-Yi Yang[1] · Chengli Li[1,2] · Peilun Hu[1,2] · Fang Yang[4] · Jiaju Lu[3] · Yin-Yuan Huang[1] · Hui Wu[1] · Qiong Wu[4] · Yongwei Pan[2] · Xiumei Wang[1,5]

Abstract

The effective and safe healing of chronic wounds, such as diabetic ulcers, presents a significant clinical challenge due to the adverse microenvironment in the wound that hinders essential processes of wound healing, including angiogenesis, inflammation resolution, and bacterial control. Therefore, there is an urgent demand for the development of safe and cost-effective multifunctional therapeutic dressings. Silicon nitride, with its distinctive antibacterial properties and bioactivities, shows great potential as a promising candidate for the treatment of chronic wounds. In this study, a silicon nitride-incorporated collagen/chitosan nanofibrous dressing (CCS) were successfully fabricated using the solution blow spinning technique (SBS). SBS offers compelling advantages in fabricating uniform nanofibers, resulting in a three-dimensional fluffy nanofibrous scaffold that creates an optimal wound healing environment. This blow-spun nanofibrous dressing exhibits excellent hygroscopicity and breathability, enabling effective absorption of wound exudate. Importantly, the incorporated silicon nitride within the fibers triggers surface chemical reactions in the aqueous environment, leading to the release of bioactive ions that modulate the wound microenvironment. Here, the CCS demonstrated exceptional capabilities in absorbing wound exudate, facilitating water vapor transmission, and displaying remarkable antibacterial properties in vitro and in a rat infected wound model (up to 99.7%, 4.5×10^7 CFU/cm² for *Staphylococcus aureus*). Furthermore, the CCS exhibited an enhanced wound closure rate, angiogenesis, and anti-inflammatory effects in a rat diabetic wound model, compared to the control group without silicon nitride incorporation.

Keywords Chronic wound · Antibacterial dressing · Silicon nitride · Solution blow spinning · Angiogenesis

---

Pengchao Ma Chun-Yi Yang and Chengli Li contributed equally to the work.

✉ Xiumei Wang
wxm@mail.tsinghua.edu.cn

1 State Key Laboratory of New Ceramics and Fine Processing, Key Laboratory of Advanced Materials, School of Materials Science and Engineering, Tsinghua University, Beijing 100084, China

2 Department of Orthopedics, School of Clinical Medicine, Beijing Tsinghua Changgung Hospital, Tsinghua University, Beijing 102218, China

3 School of Materials Science and Engineering, Zhejiang Sci-Tech University, Hangzhou 310018, China

4 MOE Key Laboratory of Bioinformatics, Center for Synthetic and Systems Biology, School of Life Sciences, Tsinghua University, Beijing 100084, China

5 Center for Biomaterials and Regenerative Medicine, Wuzhen Laboratory, Tongxiang 314500, China

Introduction

Chronic wounds, such as diabetic foot ulcers (DFUs), pose a significant global health challenge for modern society, affecting millions of patients worldwide annually. For instance, DFUs afflict up to 25% of individuals with diabetes and result in over 1 million amputations each year, carrying extensive economic and social implications [1]. Not only that, the increasing prevalence of diabetes and the high rates of vascular diseases imply a tendency for an increasing incidence of chronic ulcers. Chronic wounds do not undergo the normal process of wound healing and are typically characterized by an excessive expression of pro-inflammatory factors, high levels of reactive oxygen species (ROS), and matrix metalloproteinases (MMPs). Consequently, the extended inflammatory microenvironment disrupts revascularization, epithelialization, and controlled cytokines secretion in the

area of chronic wounds [2, 3]. Impaired angiogenesis leads to a reduced supplement of nutrition and growth factors in the chronic wound area. Numerous studies have demonstrated that dressings promoting angiogenesis and reducing inflammation play a crucial role in wound closure and the prevention of scarring [4–8]. Moreover, more than 90% of instances in the context of chronic wounds are accompanied by bacterial infections due to abnormal inflammatory processes and immune system responses, which, in turn, exacerbate inflammatory responses, impede the processes of re-epithelialization and collagen synthesis, and ultimately prolong the wound healing process. Therefore, modulating the inflammatory microenvironment and controlling infection are often indicated in the management of chronic wound healing [9].

Nowadays, a wide range of therapeutic methods have been successfully developed and applied in the treatment of various types of chronic wounds, such as negative pressure wound therapy, hyperbaric oxygen therapy, pharmacologic therapy (drugs, growth factors, genes, or stem cells), skin substitutes, and dressing therapy [10, 11]. Among these, bio-multifunctional dressings are considered powerful tools in treating chronic wounds to protect the wound bed, provide bioactivities, and serve as a matrix for tissue regeneration. Many biomaterial-based systems in the form of films, hydrogels, nanofibrous textiles, and porous scaffolds are extensively used, including collagen, chitosan, fibrin, and synthetic polymers [12–18]. In particular, nanofibrous dressings, with a structure that mimics the natural extracellular matrix (ECM), suitable porosity, and water vapor transmission ratio for absorbing excessive exudate, facilitating oxygen transmission and moisture management, show great potential in creating a favorable physiologic microenvironment for chronic wound healing [19, 20]. Furthermore, antibacterial agents like silver nanoparticles, metal oxide nanoparticles, antibiotics, and bioactive molecules such as growth factors and cytokines are commonly used to confer unique biofunctions to the dressings. However, the incorporation of bioactive components, despite their promising antimicrobial, anti-inflammatory, or angiogenic activities, is limited in clinical applications due to concerns such as drug resistance and biosafety issues. Therefore, there is an urgent need to develop innovative wound dressings that are not only cost-effective but also highly efficient and safe.

Silicon nitride (Si_3N_4) is a well-established conventional bioceramic that has been extensively studied and utilized in various biomedical applications due to its excellent biocompatibility and mechanical properties [21]. Previous studies have specifically demonstrated that Si_3N_4 exhibits broad-spectrum antimicrobial activity against a wide range of microbial strains, including the instantaneous inactivation of SARS-CoV-2 [22]. The antimicrobial property of Si_3N_4 is attributed to its surface chemical reaction with the surrounding liquid environment. The ammonium ions (NH_4^+) or ammonia (NH_3) produced by this reaction are oxidized into active nitrogen species that penetrate the cell wall of gram-positive bacteria, impairing the DNA/RNA and inhibiting bacterial proliferation. In the case of gram-negative bacteria, active nitrogen species combine with the lipopolysaccharide of the cell membrane, creating osmotic pressure that ultimately leads to bacterial rupture [23]. Therefore, unlike antibiotics, silicon nitride does not develop significant drug resistance. Besides its antibacterial properties, silicon nitride has also been reported to possess bioactivities, including angiogenic and anti-inflammatory capabilities. For example, NH_4^+/NH_3 has been shown to stimulate collagen synthesis in human osteoblasts and promote fibroblast proliferation [21, 24, 25]. Silicate ions (SiO_4^{4-}) have also been demonstrated to promote angiogenesis during processes induced by silicate bioceramics [26]. The use of an appropriate concentration of silicate ions can induce angiogenesis by increasing the gene expression of proangiogenic cytokine receptors and up-regulating downstream signaling events. The presence of silicon element enhances the activity of antioxidant enzymes, including superoxide dismutase (SOD) and catalase (CAT), thereby facilitating the inhibition of ROS formation [27]. Nonetheless, the effectiveness of Si_3N_4 in soft tissue repair has not been adequately assessed thus far. Therefore, we propose, for the first time, the incorporation of silicon nitride particles into a nanofibrous fabric dressing, which provides a straightforward and safe approach to enhance the antibacterial, angiogenic, and anti-inflammatory properties for chronic wound healing (Fig. 1).

To meet the demands of safety and efficiency, we employed collagen and chitosan as the main components for fabricating a scaffold incorporated with Si_3N_4 particles. Collagen and chitosan are widely recognized as conditional and high-safety biomaterials, making them ideal choices for biomedical applications. Collagen is a widely used biomacromolecule in skin regeneration and wound healing due to its low immunogenicity, good biocompatibility, hemostatic properties, and promotion of cell adhesion and proliferation. Most commercial wound dressings, such as Integra®, DermaMatrix®, and Biopad® that are widely used worldwide contain collagen, indicating the safety and cost-effectiveness of collagen-based products. Collagen also plays a role in immunity, and it affects the process of protein synthesis and the release of growth factors and inflammatory factors in the ECM. The porous structure of collagen scaffolds can provide mechanical support for cell migration and regeneration [28, 29]. Chitosan is a renewable natural alkaline polysaccharide with desired moisturizing and adsorption performance, making it widely used in biomedicine due to its acceptable biocompatibility and biodegradability [30]. Moreover, chitosan is also an excellent biologic additive that helps to stop bleeding and inhibit the microorganism [31–33]. Based on
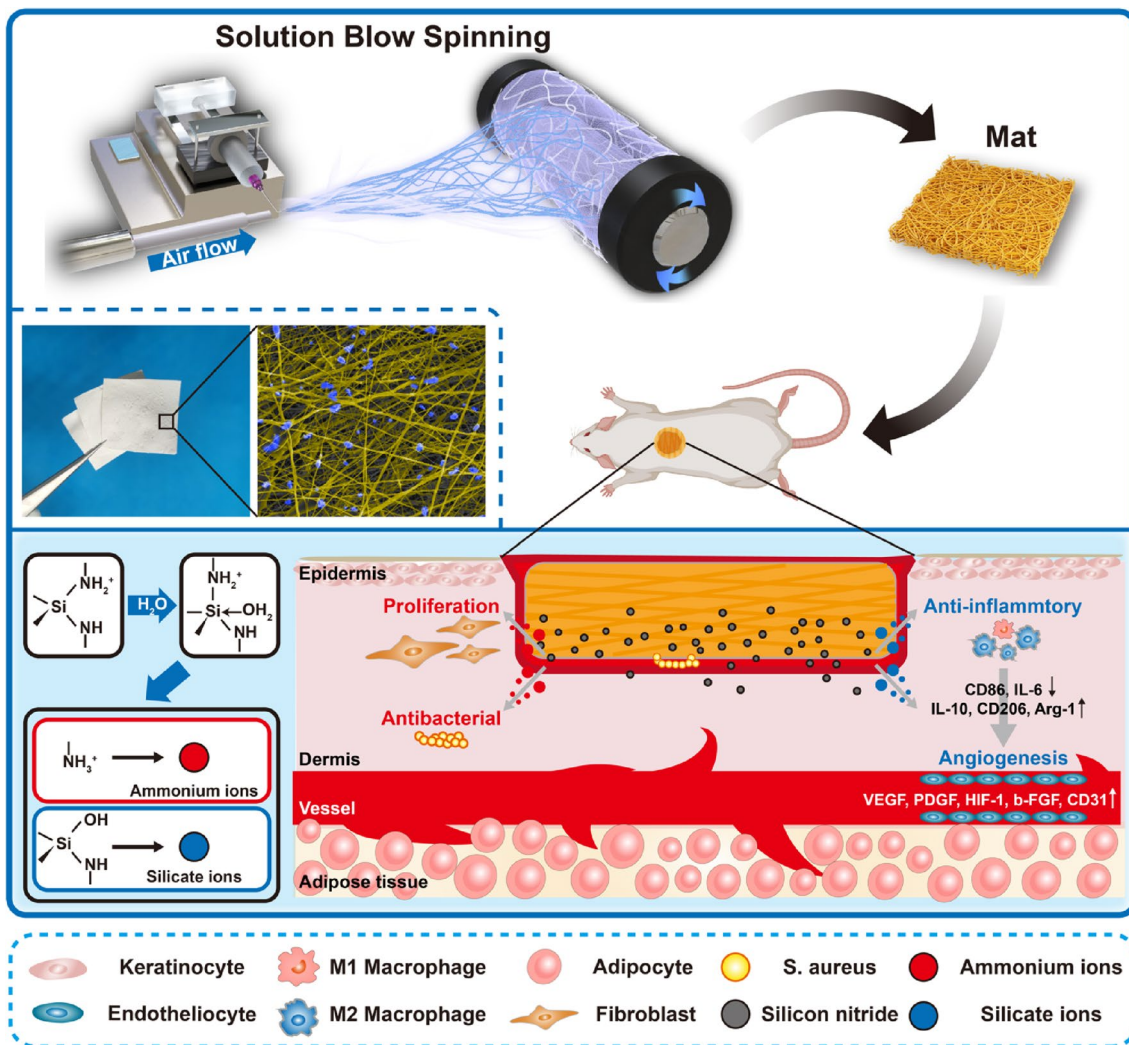
Fig. 1 Schematic illustration for the blow-spinning process of Si_3N_4-incorporated collagen/chitosan dressing with the antibacterial, anti-inflammatory, and angiogenesis properties in the wound healing process

the situations mentioned above, collagen serves as the fundamental matrix in the dressing, while chitosan is incorporated as an ingredient to enhance water absorption capacity and provide antibacterial properties.

In this study, the solution blow-spinning technique (SBS) was applied to fabricate a silicon nitride-incorporated collagen/chitosan nanofibrous dressing (CCS). In recent years, SBS has become a highly attractive method for producing nanofibrous textiles. In comparison to electrospinning, which utilizes high-voltage electric fields as the driving force, SBS offers advantages such as enhanced security, the ability of large-scale production, and exceptional product stability [34]. Moreover, the reduced number of process requirements and variables enables SBS to excel in commercial dressing preparation. Here, we expected that CCS will possess an excellent moisture absorption ratio, efficient antibacterial properties, and repair-promoting ability via

regulating inflammation and angiogenesis. The physiochemical properties, in vitro *and* in vivo antibacterial activity, and promotion of chronic wound healing of CCS were assessed.

Experimental Section

Materials

Collagen (type I, bovine origin) was purchased from Collatech, Inc. (Hebei, China). Chitosan (M_w 10,000–20,000) was purchased from Aoxing Biotechnology, Inc. (Zhejiang, China). Si_3N_4 particles were donated by Cixing New Materials, Inc. (Qingdao, China). Ethanol was purchased from Sinopharm Group Chemical Reagent Co., Ltd. (China). Acetic acid, 1-ethyl-3-(3-dimethyl aminopropyl) carbodiimide (EDC), *N*-hydroxysuccinimide (NHS), and

glutaraldehyde (GA) were purchased from Macklin Biochemical Co., Ltd. (Shanghai, China). RAW264.7 (CL-0190), HUVECs (CL-0122), DMEM culture medium, DMEM culture medium without L-glutamine, HUVECs special culture medium, and Phosphate-Buffered Saline (PBS) were obtained from Procell Life Science & Technology Co., Ltd. (Wuhan, China). Lipopolysaccharide (LPS) was purchased from Invivogen, Inc. (US).

Preparation of Blow-Spun Nanofibrous Dressing

The solution blow-spinning technique for the production of collagen-Si_3N_4 textile is shown in Fig. 1. The equipment includes three main parts: an airflow system (air pump), a discharge system (precision push pump, syringe), and a collection system (roller, controller). During the process of preparation, the discharge system precisely pushes the solution into the syringe. Subsequently, the steady pressure airflow blow-spins the solution into fibers, which are collected by the roller covered with a polytetrafluoroethylene film that rotates at a constant speed under the control of a controller. In this study, we have prepared collagen mat (COL), collagen/chitosan composite mat (CC), and CC mat loaded with 5% and 10% Si_3N_4 (CCS5 and CCS10, respectively).

To prepare the spinning solution for COL and CC, 1.5 g collagen with or without 0.1 g chitosan was dissolved in 10 mL of 40% acetic acid. To prepare CCS, different content of Si_3N_4 particles (0.5 and 1.0 g, for CCS5 and CCS 10, respectively) was added into the collagen/chitosan spinning solution. After stirring at room temperature for 24 h, the mixture was then loaded into a syringe with a needle with an inner diameter of 0.26 mm and ejected at a constant flow rate of 3.50 mL/h using a micro-infusion pump. The fibers were generated by blow-spinning the mixed solution using steady-pressure airflow under the pressure of 0.1 MPa and collected using a roller covered with polytetrafluoroethylene film. Here, a consistent volume of spinning solution (10 mL) in different mats were utilized to ensure similar thickness, with an average thickness of the blow-spun nanofibrous mat ranging from 0.42 to 0.47 mm.

EDC/NHS solution was used for crosslinking the blow-spun mats. EDC and NHS were dissolved in 90% ethanol solution at a concentration of 20 and 10 mM, respectively. The mats were soaked in the EDC/NHS solution for 24 h of crosslinking, then washed three times with ethanol and deionized water in turn, and finally dried in a vacuum freeze dryer (FD-1A-50, Beijing Biocool Instrument Co., Ltd., China). Following preparation, the mats were carefully arranged in a dish, sealed, and subsequently stored in a dryer to ensure their optimal condition prior to usage.

Characterizations of CCS

The microstructure of the mats was observed by a field emission electron microscope (SEM; Merlin, Zeiss, Germany) and transmission electron microscope (TEM; FEI, US). For SEM imaging, the films before and after crosslinking were sputter-coated with a 10 nm platinum alloy and examined at a voltage of 15 kV. For TEM imaging, the fibers were collected in the process of blow-spinning over a carbon-coated copper grid and then examined after drying at the voltage of 200 kV.

Fourier transform infrared spectroscopy (FTIR; Thermo Fisher, US) and ^1H NMR (Stanley Electric Co., Ltd., Japan) were used to confirm the chemical structure and crosslinking of the CC mats. The CC mats were treated with EDC/NHS or glutaraldehyde (GA) before testing. For GA crosslinking, samples were placed on top of the 2.0% (v/v) GA solution for 24 h at room temperature, followed by sufficient washing with deionized water to remove excess reagents. The recording wavenumber range of FTIR was set to 500–4000 cm^{-1}. The tested samples were individually soaked in D_2O, and the resulting solutions were subsequently transferred into nuclear magnetic tubes for conducting ^1H NMR tests. X-ray diffraction (XRD; Rigaku, Japan) was used to confirm the crystal structure of Si_3N_4 as a component of the dressing. The scan range was set from 0°–90°.

Thermogravimetric analysis (TGA; Q5000IR, TA Instrument, China) was used to analyze the inorganic content of blow-spun mats. The temperature range was set from 25 to 700 °C with a 10 °C/min heating rate.

Inductively coupled plasma optical emission spectrometer (ICP-OES; IRIS Intrepid II, Thermo, US) was utilized to investigate the silicate ions release. CCS10 were immersed in distilled water and agitated on a shaker at 37 °C. On days 1, 2, and 5, the supernatant was collected for analysis ($n=3$).

Water Vapor Transmission Rate Measurement

The water vapor transmission rate measurement was conducted following the method previously established [35]. COL, CC, CCS5, and CCS10 were tightly adhered to the mouths of 15 mL-centrifuge tubes containing 5 mL deionized water, and placed in a 37 °C biochemical incubator for 12 h to ensure the process of water vapor transmission reached equilibrium. The area (S) of the centrifuge tube was measured, and the total weight of the dressing and centrifuge tube (M) was weighed at 0, 0.5, 1, 1.5, 2, 4, and 12 h ($n=5$). A weight-time curve was plotted to determine the slope of transmission, and the water vapor transmission rate (WVTR) was calculated by the formula (1).

$$\text{WVTR (g m}^{-2}\text{ day}^{-1}) = \text{Slope}/S \times 24 \tag{1}$$

Moisture Absorption Rate Measurement

The method of measuring moisture absorption rate was adopted from a previous research [12]. Samples of COL, CC, CCS5, and CCS10 were cut into pieces (2×2 cm) and weighed (W_1). They were soaked in 3 mL PBS at 25 °C. At the time of 0.5, 1.5, 2, 4, and 12 h, the samples were carefully removed from the PBS and any residual liquid was absorbed using filter paper. The weight of the samples after absorption was measured (W_2). The moisture absorption ratio (MAR) was calculated by the formula (2) ($n = 5$).

$$MAR (\%) = (W_2 - W_1)/W_1 \times 100 \tag{2}$$

The Physicochemical Properties of Si_3N_4 Particles

The physicochemical properties of Si_3N_4 particles were evaluated in vitro. The particle size distribution was analyzed by a laser particle size distribution instrument (Mastor2000, Malvern, England). The concentrations of ammonium ions and silicate ions released from the Si_3N_4 particles in the aquatic environment were determined using ion chromatography (IC; 761 Compact, Metrohm, Switzerland) and ICP-OES, respectively. The Si_3N_4 particles were dispersed in distilled water and agitated on a shaker at 37 °C. On days 1, 2, and 5, the supernatant was collected for analysis ($n = 3$).

Cell Culture

L929, HUVECs, and RAW264.7 cells were used for in vitro evaluations. L929 and RAW264.7 cells were cultured in DMEM medium, and HUVECs cells were cultured in HUVECs special culture medium. The cells were cultured at 37 °C in 5% CO_2, and the medium was changed every other day. All samples were sterilized by ^{60}Co irradiation (0.05 Gy) or 75% ethanol.

In Vitro Biocompatibility of Si_3N_4 Particles

L929 cells were used to evaluate the biocompatibility of Si_3N_4 particles on cell proliferation. To obtain the leaching medium, Si_3N_4 particles were added to DMEM without L-glutamine at concentrations of 5000 µg/mL and shaken for 24 h. The medium was then centrifuged at 10,000 rpm for 10 min and subsequently sterilized by a 0.22 µm filter. Cells were seeded at the density of 1×10^3 cells per well in a 96-well culture plate and incubated for 12 h. The medium was then replaced with the DMEM (Control), DMEM without L-glutamine (Blank), leaching medium diluted to 10% (Si_3N_4 (10%)), leaching medium diluted to 50% (Si_3N_4 (50%)), and undiluted leaching medium (Si_3N_4 (100%)). The cell viability was monitored by Cell Counting Kit-8 assays (CCK-8; Dojindo, Japan) after further incubation for 24 h.

In Vitro Anti-Inflammatory and Angiogenesis Effect of Si_3N_4 Particles

RAW264.7 cells were used to evaluate the anti-inflammatory effect of Si_3N_4 particles in vitro. The cells were cultured in T-25 flasks with the medium containing different concentrations of Si_3N_4 particles (5, 50, 500, 5000 µg/mL) at a density of 5×10^5 cells per flask. After 4 days of incubation, the RNAs of RAW264.7 were isolated using RNAsimple Total RNA Kit (Tiangen, China). Next, the FastKing RT Kit (Tiangen, China) was used for cDNA reverse transcription, and the CFX Connect Real-Time PCR Detection System (BIO-RAD, US) was used to perform real-time PCR (RT-PCR). GAPDH was used as a reference gene, and the $2^{-\Delta\Delta CT}$ method was used for analyzing the expression of inflammatory-related genes including interleukin-6 (IL-6), cluster of differentiation 86 (CD86), interleukin-10 (IL-10), arginase-1 (Arg-1), and mannose receptor C-type 1 (CD206) ($n = 3$).

HUVECs were utilized to investigate the potential angiogenesis effect of Si_3N_4 particles in vitro. Briefly, HUVECs were cultured in T-25 flasks with different concentrations of Si_3N_4 particles (5, 50, 500, 5000 µg/mL) at a density of 5×10^5 cells per flask. After 4 days of incubation, the RNAs of HUVECs were extracted, and RT-PCR was performed after reverse transcription. GAPDH was used as a reference gene, and the $2^{-\Delta\Delta CT}$ method was employed to analyze the expression of angiogenesis-related genes including vascular endothelial growth factor (VEGF), platelet-derived growth factor (PDGF), platelet endothelial cell adhesion molecule-1 (CD31), basic fibroblast growth factor (bFGF), and hypoxia-inducible factor-1 (HIF-1) ($n = 3$). The sequences of related primers were listed in the supplement (Table S1).

To further evaluate the effect of macrophage on regulating cell angiogenesis, RAW264.7 cells were co-cultured indirectly with HUVECs using a transwell system. The HUVECs were cultured in a 24-well plate with an Insert (Corning, US) in it that contained RAW264.7 cells with or without Si_3N_4 particles. Three experimental groups were established: (1) only Si_3N_4 particles, (2) only RAW264.7, and (3) RAW264.7 treated with Si_3N_4 particles in the insert. After incubation for 4 days, the level of VEGF in the supernatants was measured using an ELISA kit. The experiment was repeated five times ($n = 5$).

In Vitro Biocompatibility of CCS

L929 cells and HUVECs were utilized to evaluate the cytotoxicity of the CCS. Briefly, the mats (COL, CC,

CCS5, CCS10) were cut into circles (1.5 cm in diameter) and placed in the 24-well plate. The samples were then sterilized by ^{60}Co irradiation at 5 Mrad. L929 cells were seeded onto the samples at the density of 2×10^5 cells per well. After incubation for 24 h, the medium was discarded, and the Live/Dead staining was performed. To prepare the working solution, 40 μg Calcein-AM and 60 μg Propidium Iodide (Sigma, US) were dissolved in 10 mL PBS. The samples were then incubated with 500 μL working solution at 37 °C for 40 min. After staining, the samples were washed 3 times with PBS to terminate excessive staining and then observed using a laser confocal microscope (LSM980 Airyscan2, Zeiss, US) [36]. The experimental details of HUVECs are available in the Supplementary Material.

L929 cells were used to evaluate the influence of blow-spun mats on cell proliferation. The mats (COL, CC, CCS5, CCS10) were cropped into round pieces (1.2 cm in diameter) and placed in the wells of a 24-well culture plate. Seeded L929 cells were then added at a density of 2×10^4 cells per well. The cell viability of L929 was monitored by CCK-8 assays at days 1, 3, and 5 ($n = 5$).

In Vitro Antibacterial Ability of CCS

To investigate the antibacterial ability, the mats (1.2 cm in diameter) of COL, CC, CCS5, CCS10 were placed in the wells of a 48-well plate. Then, 50 μL suspension of *S. aureus* or *E. coli* (4×10^5 CFU/mL) was added to the samples.

After incubation for 12 h at 37 °C, 500 μL bacterial medium was added to each well and further incubated for another 12 h. Next, 100 μL bacterial suspension, diluted by a factor of 10^5, was uniformly inoculated on LB plates and incubated for 24 h at 37 °C. The experiments were performed in triplicate ($n = 3$).

In Vitro Anti-Inflammatory and Angiogenesis Effect of CCS

Untreated RAW264.7 cells, LPS-activated RAW264.7 cells, and HUVECs were used to evaluate the anti-inflammatory/angiogenesis effect of CCS in vitro. RAW264.7 cells were treated with 1 μg/mL LPS for 24 h to obtain LPS-activated RAW264.7 cells. The mats were added to medium and incubated for 48 h at 37 °C. The medium was then centrifuged at 10,000 rpm for 10 min and subsequently sterilized by a 0.22 μm filter. The cells were seeded in a 6-well culture plate at a density of 5×10^4 cells per well, after incubation for 12 h, the medium was replaced with the leaching medium (COL, CC, CCS5, CCS10). After 3 days of incubation, the RT-PCR was performed.

In Vivo Evaluations on the Antibacterial Ability and Chronic Wound Healing

In our study, two animal models, namely the infected wound model and the diabetic wound model, were utilized to separately assess the antibacterial efficacy and wound healing potential of CCS dressings, avoiding the potential mutual interference of infection and diabetes.

The animal studies were performed in strict accordance with the Guide for the Care and Use of Laboratory Animals of the National Institutes of Health and was approved by the Institutional Animal Care and Use Committee of Tsinghua University (Beijing, China). The laboratory animal facility has been accredited by the Association for Assessment and Accreditation of Laboratory Animal Care International (AAALAC).

To evaluate the short-term antibacterial ability of the dressing, the experiment on the rat infected wound model was performed referring to previous research [12]. Male SD rats weighing between 180–220 g were used to evaluate the antibacterial ability of CCS. The rats were divided into five groups consisting of thirteen rats each: Control, COL, CC, CCS5, and CCS10. After anesthesia, full-thickness cutaneous wounds (1.5 cm in diameter) were created on the backs of rats, and anti-contraction rings were used to eliminate the effect of the contraction of the flesh membrane of the rats. Next, 200 μL *S. aureus* suspension (4×10^8 CFU/mL) was added to create the wound infection model. Then, wounds were treated with COL, CC, CCS5, and CCS10 (1.5 cm in diameter), and bandages were used to tie the wound area after putting one layer of polyurethane dressing on the samples to manage the wounds more conveniently. The dressings were changed every 3 days, and wound tissues were collected for hematoxylin and eosin (H&E) and Giemsa staining on days 6 and 12 ($n = 5$). To investigate the short-term antibacterial ability, the rats were sacrificed, and the wound tissues were collected and weighed on day 3. The tissues were homogenized in 500 μL PBS solution at 4 °C with a high-speed tissue grinder (Tiangen, China). The tissue suspension was centrifuged at 2500 rpm at 4 °C for 5 min, and 100 μL of supernatant was inoculated on LB plates after 1000 times dilution. LB plates were incubated for 24 h at 37 °C for CFU counting ($n = 3$).

The ability of CCS to promote chronic wound healing was evaluated using a rat diabetic wound model. Male SD rats weighing between 180–220 g were used to evaluate the antibacterial ability of CCS. The rats were divided into five groups consisting of ten rats each: Control, COL, CC, CCS5, and CCS10. Firstly, the diabetic rat model was established by intraperitoneal injection of streptozocin (STZ), and the blood glucose of rats was monitored after 5 days. Rats with blood glucose above 16.7 mM were regarded as diabetic rat models [37]. Then full-thickness cutaneous wounds (1.5 cm

in diameter) were created on the backs of rats under anesthesia, and anti-contraction rings were used to eliminate the effect of the contraction of the flesh membrane of the rats. The wounds were treated with COL, CC, CCS5, and CCS10 (1.5 cm in diameter) and put one layer of polyurethane dressing on the samples, and tied the wound area by a bandage. The wound tissues were collected for hematoxylin and eosin (H&E) and Masson staining on weeks 4 ($n=5$).

Moreover, immunofluorescence staining was conducted to observe the hair follicle structure using K14 as a marker. In addition, CD68, CD206, and iNOS staining were performed to assess the macrophage phenotype. Moreover, CD31 and α-SMA staining were carried out to observe the newly formed blood vessels.

Statistical Analysis

The Prism 9 software (GraphPad, US) and Origin 9 (OriginLab, US) were used for data analyses. The images were analyzed by ImageJ (HHS, US). One-way ANOVA was performed during the statistical analysis with triple data at least. A value of $P < 0.05$ is considered statistically significant, and the statistically significant are indicated as *$P < 0.05$, **$P < 0.01$, ***$P < 0.001$.

Results and Discussion

The Physiochemical Properties of CCS

Considering the factors of spinnability, nanofiber continuity, and homogeneity, the optimal ratio of collagen to chitosan was determined as 15:1 (w/w) for subsequent experimental investigations (Fig. S1). In the blow-spinning process, chitosan played a pivotal role by increasing the viscosity of the spinning solution, resulting in improved dispersion and stability of the silicon nitride particles and enhanced spinnability. Moreover, the concentration of Si_3N_4 nanoparticles had obvious influences on the spinnability and the mechanical properties of the blow-spun nanofiber mat. In this study, no precipitation or aggregation of Si_3N_4 particles with less than 15% in the spinning solution was observed throughout the entire blow-spinning process, as indicated by its appearance, thereby ensuring a consistent and reliable fabrication process. Because the mat containing 15% Si_3N_4 showed a dramatic decrease in mechanical properties (Fig. S2), 5% and 10% Si_3N_4 were utilized for further evaluations. As shown in SEM images (Fig. 2a), all the samples could form uniform and interwoven nanofibers by blow-spinning. The inclusion of Si_3N_4 particles did not cause any needle blockage or compromise the integrity of the nanofiber network during the spinning process. In addition, according to the SEM images,

the Si_3N_4 particles were well embedded in the collagen/chitosan fibers and did not detach from them, indicating their good stability in the nanofibers. The fiber diameters primarily fell within the range of 200–500 nm, with a substantial number of fibers measuring below 300 nm after the incorporation of silicon nitride (Fig. 2e). The TEM images clearly showed the encapsulation of particles in the CCS5 and CCS10 fibers (Fig. 2c). XRD and TGA analyses were conducted to confirm the successful composite of collagen fiber and Si_3N_4 particles in CCS5 and CCS10. The XRD spectra of CCS5 and CCS10 exhibited typical diffraction peaks associated with the crystal structure of β-Si_3N_4 particles, with peak intensity increasing proportionally to the content of Si_3N_4 particles (Fig. 2f). The content of Si_3N_4 particles in the mats was accurately calculated according to TGA results (Fig. 2g), with 26.2% (w/w) in CCS5 and 39.9% (w/w) in CCS10, which closely matched the theoretical values of 23.8% and 38.5%, respectively. These results suggest that the collagen/chitosan/Si_3N_4 solution can be effectively and reliably spun into a nanofibrous mat using SBS.

In addition, as shown in Fig. 2b, chemical crosslinking had no significant impact on the primary structure of the nanofiber. After crosslinking, the CCS retained its fibrous mat structure in water, whereas the un-crosslinked CCS lost its structural integrity when exposed to water (data not shown). FTIR assay further confirmed the successful crosslinking. It was observed that both EDC/NHS and GA crosslinking methods led to enhanced absorption peaks at 3300, 3076, 1643, 1531, and 1238 cm^{-1}, corresponding to amide A, amide B, amide I, amide II, and amide III (Fig. 2h) [38]. In addition, treatment with EDC/NHS and GA resulted in a shift of the amide A peak from 3288 cm^{-1} to 3303 and 3305 cm^{-1}. This shift can be attributed to the enhanced N–H vibration caused by the formation of newly formed amide bonds, which led to a redshift in the spectral band. The results of the ^1H NMR spectrum additionally confirmed the successful crosslinking process of the nanofibers. Two newly formed characteristic peaks were observed at 2.8 and 8.5 ppm, respectively, indicating the formation of a new amide bond (Fig. S3) [39]. Notably, due to the better crosslinking effect and weaker toxicity, EDC/NHS was chosen as the preferred crosslinking reagent for subsequent experiments.

The maintenance of a humid microenvironment is critical to promote efficient wound healing, and this process is largely influenced by the material properties of wound dressings, such as their water vapor transmission rate and moisture absorption capacity. It is well established that an optimal WVTR is essential to create a moist wound environment and prevent the accumulation of wound exudates [40]. The average WVTR of different blow-spun mats ranged from 751.76 to 865.92 g•m^{-2}•day^{-1} (Fig. 2i), which was
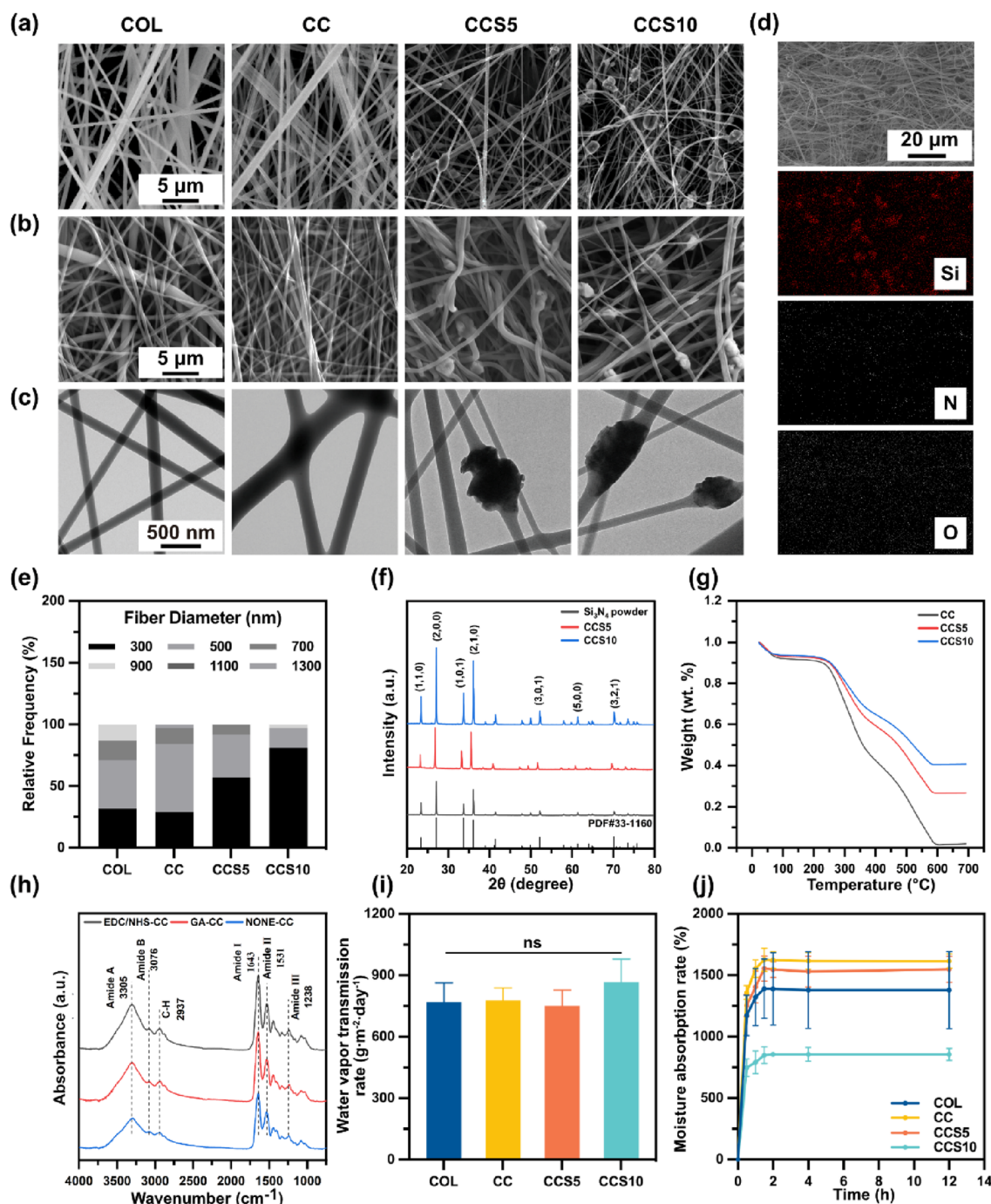
Fig. 2 The physiochemical properties of CCS. SEM images of the blow-spun nanofibers **a** before and **b** after chemical crosslinking. **c** TEM images of the blow-spun nanofibers. **d** EDX images of CCS5. **e** Relative frequency of fiber diameter. **f** XRD spectra. **g** TGA curves. **h** FTIR spectra. **i** Water vapor transmission rate. **j** Moisture absorption curves

comparable to that of the commercial wound dressings [41]. The addition of chitosan and Si_3N_4 particles had no significant impact on the WVTR.

Moisture absorption property evaluation was conducted using PBS as the test solution. As depicted in Fig. 2j, all mats reached absorption equilibrium within

2 h. Importantly, COL, CC, and CCS5 demonstrated the ability to absorb 13.8, 16.2, and 15.5 times their weight in water, respectively. The addition of chitosan enhanced the moisture absorption capabilities of the mats due to the abundant hydroxyl groups in chitosan, which formed hydrogen bonds with adjacent water molecules. The

addition of Si_3N_4 particles in CCS5 had a negligible influence on the moisture absorption capabilities, while CCS10 showed impaired moisture absorption capabilities and could only absorb 8.6 times its weight due to the increased content of Si_3N_4 particles. Despite the moisture absorption capabilities of the CCS10 mats decreasing in comparison with other mats, the saturated absorption ratio still reached 856.1%, indicating excellent capability in absorbing excessive wound exudates.

Anti-Inflammatory and Angiogenic Properties of Si_3N_4 Particles

In this study, the angiogenic and anti-inflammatory properties of Si_3N_4 particles may dominantly attribute to the release of NH_4^+ and SiO_4^{4-} from the hydrolysis of Si_3N_4 particles (Fig. 3a). The overall diameter of Si_3N_4 particles ranged from 800 to 1100 nm (Fig. 3b), providing a larger specific surface area for reaction in a liquid environment. The surface chemistry reaction of Si_3N_4 particles follows the S_N2 mechanism, in which water plays the role of a nucleophilic
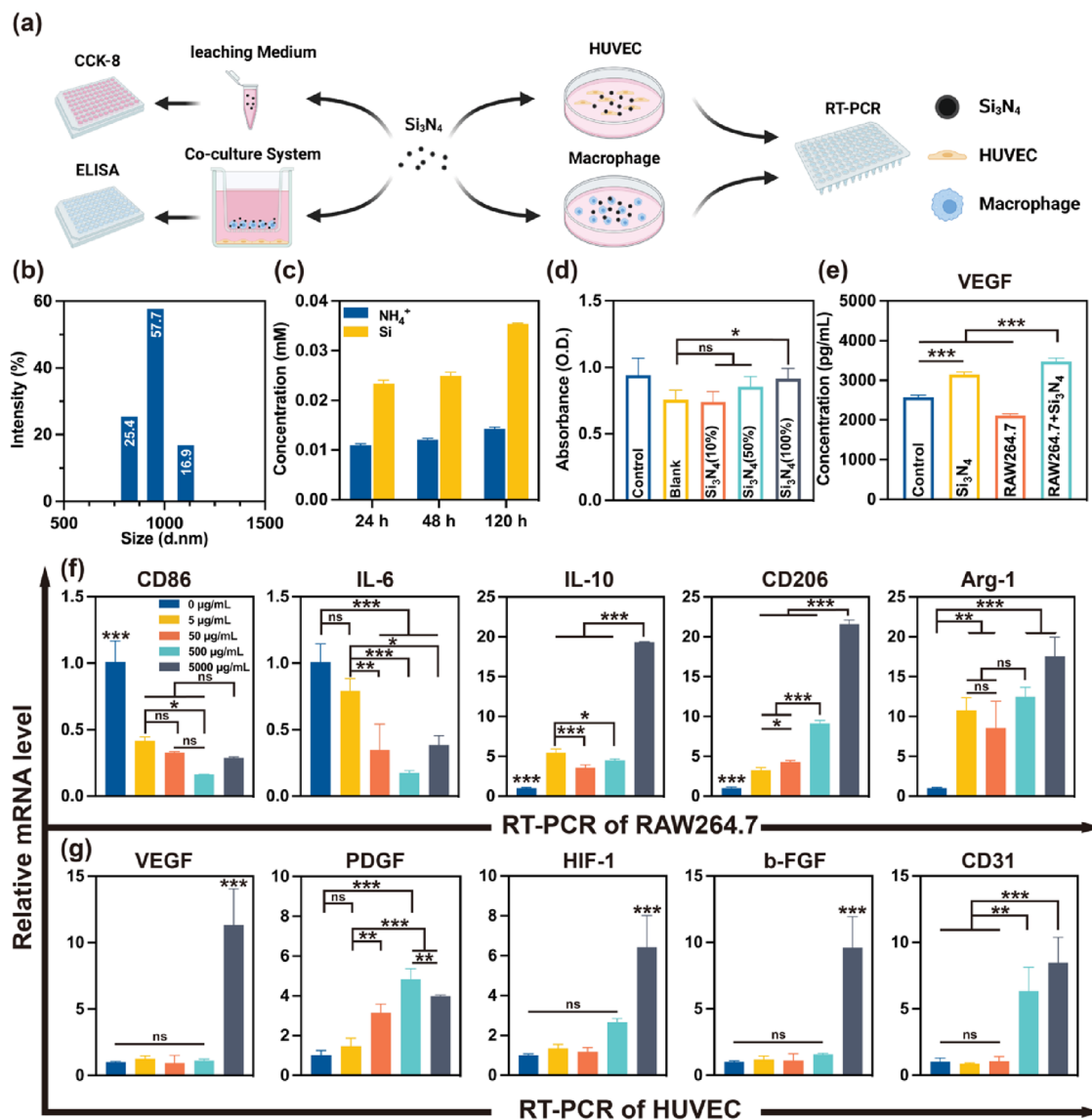

Fig. 3 Comprehensive evaluations on Si_3N_4 particles by in vitro cell culture. **a** A diagrammatic illustration on in vitro cell evaluations (Created by Biorender.com). **b** Diameter distribution of Si_3N_4 particles. **c** IC/ICP result. **d** CCK-8 result of L929 treated with Si_3N_4-leaching medium. **e** ELISA result of VEGF concentration secreted by HUVECs after co-culture with RAW264.7. **f** RT-PCR result of anti-inflammatory-related genes. **g** RT-PCR result of angiogenesis-related genes. Mean values and error bars are defined as mean and SD, respectively; *$P<0.05$, **$P<0.01$, ***$P<0.001$

agent and attacks the Si_3N_4 surface to increase energy in a fluid environment (Fig. 1). The amine dissociates from the surface sites to form NH_4^+ and SiO_4^{4-} [42, 43]. The persistent elution of NH_4^+ and SiO_4^{4-} from the Si_3N_4 particles over a period of 5 days was monitored by IC and ICP-OES, as shown in Fig. 3c. NH_4^+ can be assimilated through the glutamine synthetase/glutamate pathway as a nutrient for cells to synthesize proteins, thus promoting cell proliferation and differentiation. L929 cells were cultured with Si_3N_4 leaching medium to evaluate the influence of Si_3N_4 particles on fibroblast growth. As shown in Fig. 3d, there was a significant difference between the control group and the blank group, demonstrating the positive role of glutamine in cell proliferation [21]. With the addition of Si_3N_4 leaching medium, the viability of cells showed an upward trend. The cell viabilities of the control group and Si_3N_4 (100%) group were essentially the same, indicating the promoting effect of Si_3N_4 on fibroblast proliferation, especially in the impaired nutritional environment of the chronic wound area.

Furthermore, the effect of Si_3N_4 particles on inflammation and angiogenesis was studied at the level of genetics. As shown in Fig. 3f, the inflammatory-related gene expression of RAW264.7 including CD86 (M1 marker) and IL-6 showed the opposite decrease tendency with the increasing of Si_3N_4 particle concentration in the medium. Moreover, the expression of anti-inflammatory factor genes including IL-10, CD206 (M2 marker), and Arg-1 was upregulated as the elevation of the content of Si_3N_4 particles in the medium. All the results demonstrate that Si_3N_4 particles can effectively regulate the inflammatory environment by decreasing the macrophage phenotype ratio of M1/M2.

In addition to its effect on fibroblast proliferation and inflammation, Si_3N_4 particles also showed a significant impact on angiogenesis, as indicated by the upregulation of angiogenic-related gene expression in HUVECs (Fig. 3g). The results revealed that Si_3N_4 particles at a concentration of 500 and 5000 µg/mL significantly promoted the expression of CD31, which is an important factor in angiogenesis, while the lower concentrations of Si_3N_4 particles had little effect on CD31 expression. The expression of HIF-1 and b-FGF was also upregulated with a substantial increase of 6.4- and 9.6-fold observed in the 5000 µg/mL group, respectively. Interestingly, the mRNA level of PDGF was highly related to the concentration of Si_3N_4 particles, with a 3.1-fold increase observed at a concentration of 50 µg/mL. Overall, these findings indicate that Si_3N_4 particles have a positive effect on angiogenesis, which may be beneficial in promoting wound healing.

The result of the co-culture test further researched the role of Si_3N_4 particles in the interaction between angiogenesis and inflammatory regulation: the relative level of VEGF was elevated by 1.4-fold when treated with the RAW264.7 and Si_3N_4 particles while the value is 1.2 when treated with only Si_3N_4 particles (Fig. 3e), which demonstrated the vital, positive regulating property of Si_3N_4 particles in the interaction between angiogenesis and inflammatory regulation. In brief, these findings suggest that Si_3N_4 particles have a significant potential for promoting wound healing by regulating inflammation, promoting angiogenesis, and providing a source of nutrients for cell proliferation and differentiation.

In Vitro Biocompatibility and Antibacterial Properties of CCS

After evaluating the effect of Si_3N_4 particles on cells, we assessed the biosafety, cell proliferation promotion, and antibacterial activity of the blow-spun mats. The results depicted in Fig. 4a demonstrate that all mats displayed no cell toxicity, with a cell viability exceeding 99%. Furthermore, the leaching medium from the blow-spun mats exhibited no cell toxicity towards the endothelial cells (Fig. S4). Furthermore, the CCK-8 assay indicated that the fibroblasts showed a good proliferation tendency in the blow-spun mats leaching medium. The CCS5 and CCS10 groups showed a rising trend in absorbance at 5 days, confirming the beneficial effect of Si_3N_4 particles on cell proliferation (Fig. 4b).

Although the in vitro cell studies have demonstrated the excellent biocompatibility of the blow-spun mats, their antibacterial properties are required to be evaluated for clinical wound treatment. As depicted in Fig. 4d,e, the inclusion of chitosan and Si_3N_4 particles resulted in a substantial reduction in the survival rate of both *S. aureus* and *E. coli*. Chitosan augmented the antibacterial effect, while the Si_3N_4 particles further enhanced the performance of the mats. The survival rates of *S. aureus* in the CCS5 and CCS10 groups were only 16.4% and 3.2%, respectively. Interestingly, the Si_3N_4 particles exhibited remarkable antibacterial efficacy against *E. coli*, resulting in survival rates of merely 0.38% and 0.13% for the CCS5 and CCS10 groups, respectively. The results demonstrated the remarkable antibacterial performance of Si_3N_4 particles in the mats via the bacteria cracking by NH_4^+ produced in Si_3N_4 hydrolysis.

Furthermore, the study investigated the impact of CCS on inflammation and angiogenesis at the genetic level. To validate the bioactivity of CCS, the expression of inflammatory-related genes in untreated RAW264.7 cells was assessed using RT-PCR (Fig. S5). In addition, LPS-activated RAW264.7 cells were employed to evaluate the immunoregulatory properties of CCS. As shown in Fig. 4f, the expression of inflammatory-related genes CD86 and IL-6 in LPS-activated RAW264.7 cells exhibited a decreasing trend in COL, CC, and CCS groups. The immunomodulatory effect of COL and CC may have contributed to this outcome, with the addition of Si_3N_4 particles appearing to enhance this effect. Moreover, the expression of anti-inflammatory factor genes, especially CD206, was upregulated with the increasing content of Si_3N_4 particles
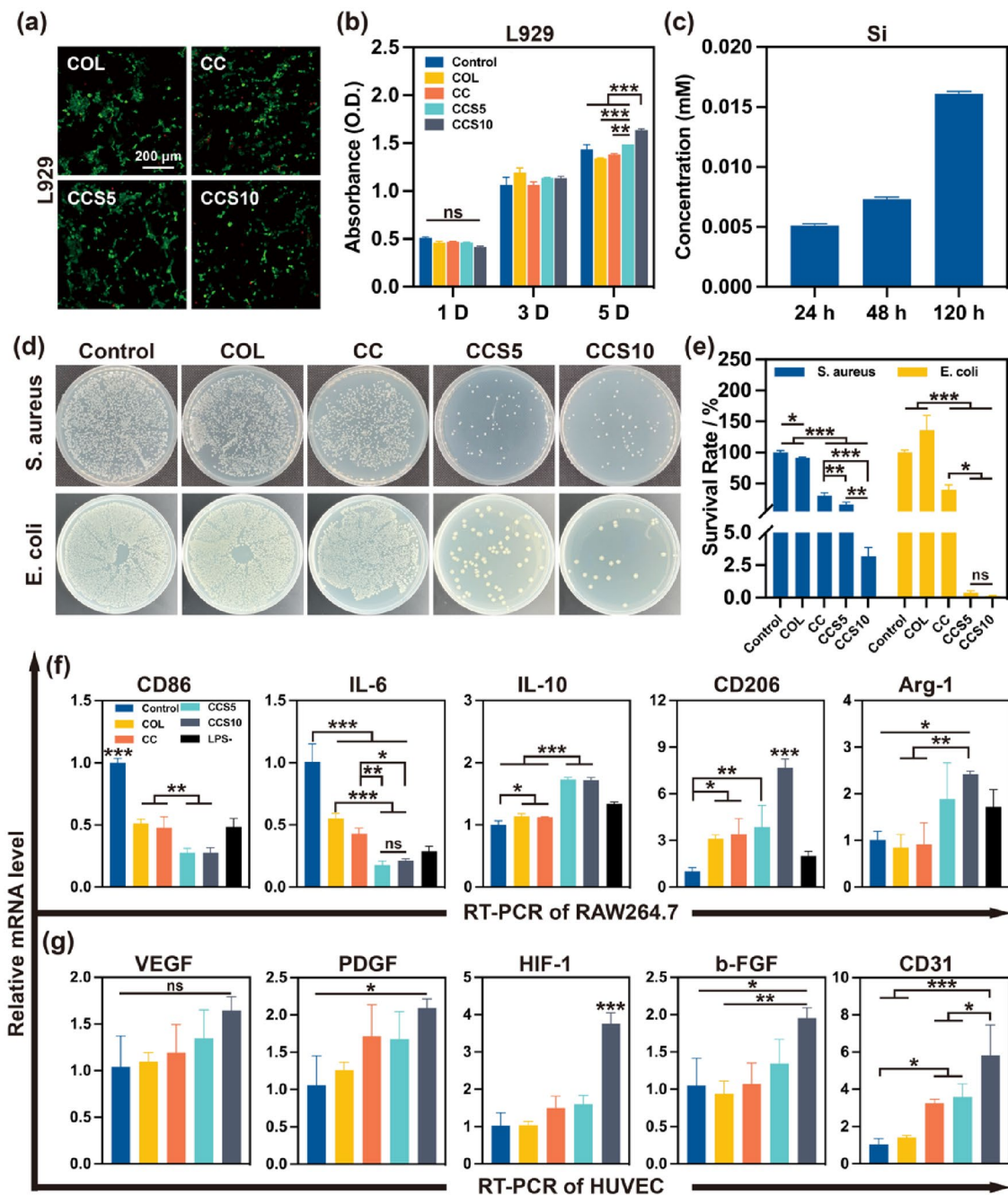
Fig. 4 In vitro biocompatibility and antibacterial properties of CCS. **a** Live/dead straining images of L929. **b** CCK-8 result of L929 treated with CCS. **c** Silicate ions concentration released from Si_3N_4 by ICP ICP-OES assay. **d** Typical morphologies of *S. aureus* and *E. coli* colonies after 24 h culture on LB plates. **e** CFU counts of *S. aureus* and *E. coli* after being treated with CCS. **f** RT-PCR result of anti-inflammatory-related genes. **g** RT-PCR result of angiogenesis-related genes. Mean values and error bars are defined as mean and SD, respectively; *$P < 0.05$, **$P < 0.01$, ***$P < 0.001$

in the medium, whereas COL and CC showed only slight changes, highlighting the significant role played by Si_3N_4 particles in anti-inflammatory responses. Moreover, the results revealed a significant impact of CCS on angiogenesis, as evidenced by the upregulation of angiogenic-related gene expression in HUVECs upon the incorporation of

Si_3N_4 particles in CCS (Fig. 4g). These bio-regulatory effects of the CCS dressing are attributed to the continuous release of ions from the silicon nitride particles, as demonstrated by the ICP-OES results (Fig. 4c) [26]. This finding is consistent with previous experimental results obtained during the validation of silicon nitride particles.

In Vivo Accelerated Wound Healing by the Antibacterial and Anti-Inflammatory Effects of CCS

After evaluating the biosafety and antibacterial performance of the CCS, the short-term and long-term antibacterial and wound healing properties were further assessed in a rat model with full-thickness cutaneous wounds infected with *S. aureus*. As demonstrated in Fig. 5a, c, all of the blow-spun mats could promote the infected wound healing. Particularly, the CCS5 and CCS10 groups were highly effective over the entire healing process, effectively absorbing exudates to maintain cleanliness around the wound and exhibiting less canker tissue. Significant differences were observed among groups on day 3, with relative wound area of 85.5% and 74.7% for CCS5 and CCS10, respectively, compared to values of 134.0%, 104.0%, and 97.1% for the Control, COL, and CC groups, respectively (Fig. 5d). To further investigate the short-term antibacterial properties of CCS, the CFU in the wound was counted after 3 days. As shown in Fig. 5b, e, COL could hardly eliminate bacteria, while CC demonstrated good antibacterial performance. The antibacterial activities of CCS5 and CCS10 are remarkable, especially CCS10, which effectively eradicated all bacteria from the wound by day 3.

The healing efficacy of CCS in the infected wounds was further investigated at the tissue level. H&E staining (Fig. 5f, g) revealed that although collagen and chitosan, as the basic composites of mats, accelerated wound closure, there were still varying degrees of necrosis and abscesses in the Control, COL, and CC groups. In contrast, the CCS5 and CCS10 groups exhibited superior antibacterial activity, and the CCS10 group showed complete healing of the ECM and hair follicles. Furthermore, Giemsa staining provided additional evidence of the remarkable antibacterial performance of CCS. On day 12, the wound tissue of the Control and COL groups exhibited abundant bacterial colonies, while the CCS5 and CCS10 groups showed minimal colonies (Fig. 5h).

In Vivo Accelerated Diabetic Wound Healing by the Anti-Inflammatory and Angiogenesis Effects of CCS

Based on the promising results of CCS in treating infected wounds, we further conducted investigations on its efficacy in treating chronic wounds in a rat diabetic wound model. The wounds were imaged weekly for up to 4 weeks. The CCS10 group showed the best healing status without visible scar (Fig. 6a). The relative wound area curve with time (Fig. 6b) showed that the healing rates of wounds in the CCS5 and CCS10 groups were much faster than those in other groups. Notably, the relative wound area of the CCS10 group was the smallest among all the groups at week 4 (Fig. 6c). The relative wound area in the CCS10 group was only 1.5%, while the mean values in the Control, COL, CC, and CCS5 groups were 17.3%, 12.9%, 10.8%, and 5.8%, respectively.

These results were confirmed by H&E and Masson's trichrome staining, which demonstrated the excellent performance of CCS in accelerating diabetic wound healing (Fig. 7a). More skin defects and cavities were found in the Control, COL, and CC groups, while the newly formed fibers in the CCS5 and CCS10 groups were denser and arranged more neatly. The collagen deposition of the Control group was only 28.3%, while the COL and CC groups elevated the mean up to over 40%, demonstrating the positive role of collagen in rebuilding the ECM (Fig. 7b, g). In comparison, more complete skin structures, fewer inflammatory cells, and more collagen fibers could be found in the CCS5 and CCS10 groups, especially in the CCS10 group.

We then performed CD68/iNOS/CD206 immunostaining, which were used as the pro-inflammatory and anti-inflammatory markers, respectively. It was observed that the relative coverage area of iNOS and CD68 (M1 marker) was higher in the wound areas of the Control, COL, and CC groups (Fig. 7c, h). This indicates that the chitosan used in our blow-spun mats did not effectively exert an anti-inflammatory effect on chronic wounds. In contrast, the CCS5 and CCS10 groups showed a lower relative coverage area of iNOS, indicating a favorable healing state with reduced inflammation. Importantly, the Si_3N_4 material exhibited remarkable immunoregulatory capacity, as indicated by a significantly larger relative coverage area of CD206 (M2 marker) in the CCS5 and CCS10 groups (Fig. 7d, i).

In addition, CD31 and α-SMA were used to label the blood vessels, and the wounds treated with CCS5 and CCS10 displayed significantly higher numbers of blood vessels than the other groups (Fig. 7e, j). Furthermore, K14 was used to label the hair follicle to evaluate the formation of mature dermal structures. As shown in Fig. 7f and Fig. S8, the hair follicles in the Control group showed a lower level of number, maturity, and completeness. For the COL and CC groups, there was an increase in the number of hair follicles, but the new hair follicle structure was still immature. In contrast, the hair follicle structure in the
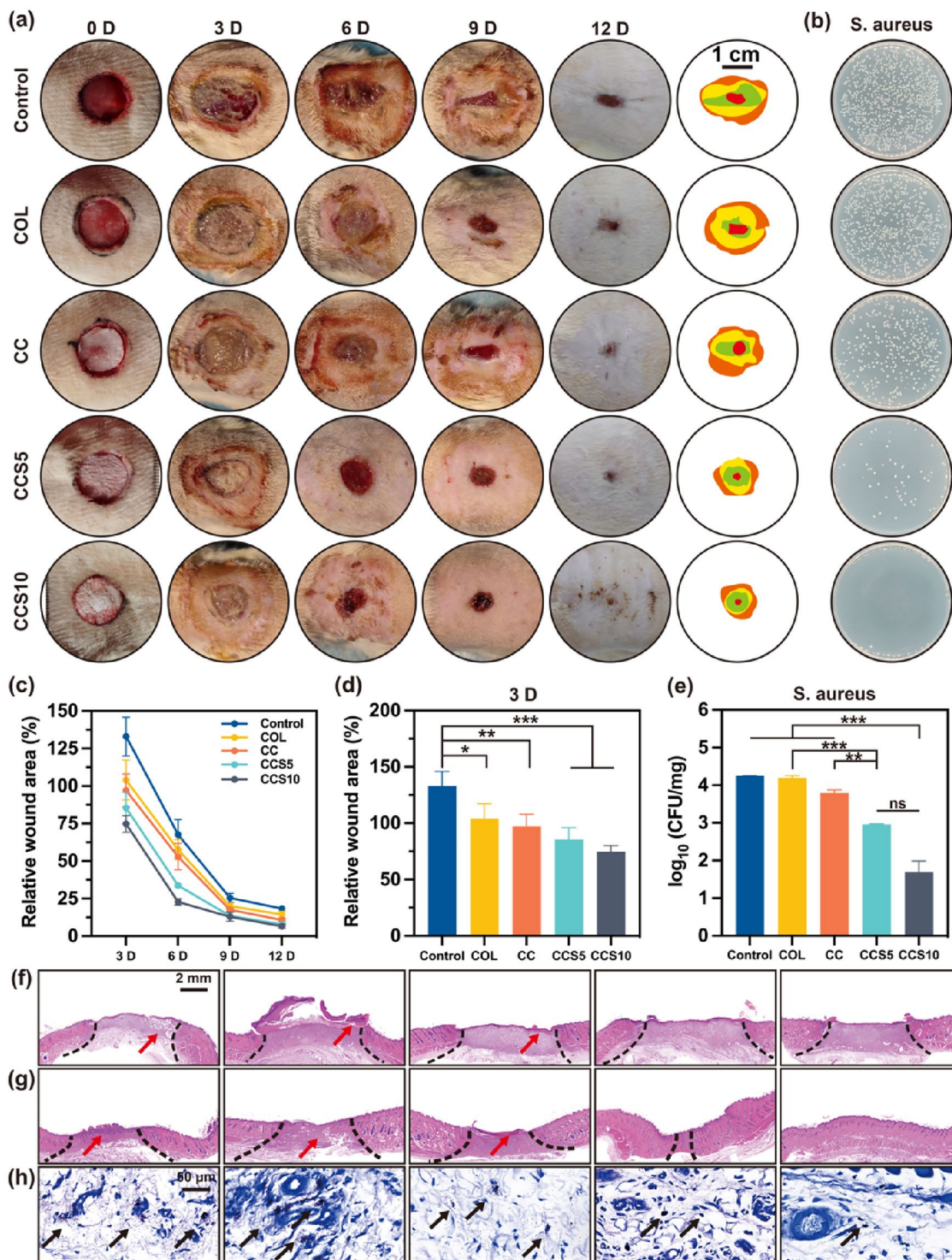
Fig. 5 Evaluation of antibacterial and anti-inflammatory properties of CCS in an infected rat wound model. **a** Images of the wound tissues with different dressings treatments at the different time points. **b, e** CFU counts of the remaining bacteria in the wound tissues after 3 days. **c, d** Corresponding relative wound area. H&E staining of the wound tissues with different dressing treatments for **f** 6 days and **g** 12 days. The tissue between the black dotted line is unhealed, the red arrow refers to the necrotic and abscesses area. **h** Giemsa staining of the wound tissues with different dressings treatments for 12 days
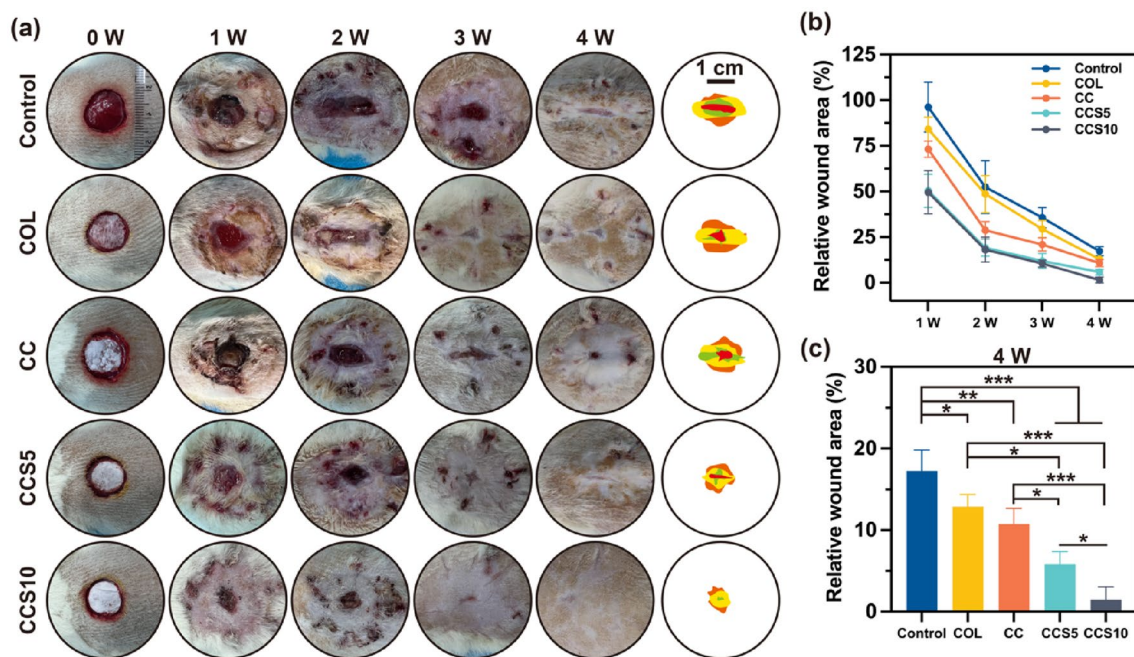
Fig. 6 Evaluation of the performance of CCS in a rat diabetic model. **a** Gross images of the wound tissues with different dressings treatments at different time points. **b, c** Corresponding relative wound areas

CCS5 and CCS10 groups appeared to be more mature, and the complete hair follicle structure was first observed in the CCS10 group. These results suggest that the promoting effects of Si_3N_4 on angiogenesis and immunoregulation contribute to the remodeling phase in the chronic wound healing process.

Discussion

Compared to electrospinning, the use of SBS offers several advantages in terms of security, stability, and scalability (Fig. S7). Dressings prepared by SBS demonstrate both cost-effectiveness and good efficiency in wound healing. The network composed of collagen/chitosan nanofibers within the dressing exhibits excellent WVTR and water absorption capacity, creating a favorable moist environment that accelerates wound closure. In general, SBS can be a rapid, stable, and cost-effective technique to fabricate nanofibrous fabrics for all kinds of biomedical applications.

In this study, the incorporation of a small amount of chitosan could enhance water retention and antibacterial properties of the blow-spun mats. However, it has been observed that chitosan has limited efficacy in regulating inflammation in vivo due to its low content. To address the issue, Si_3N_4 was introduced in blow-spun mats as a bioactive agent with combined antibacterial, anti-inflammatory, and angiogenic

activities. In vitro studies have revealed that Si_3N_4 plays a positive role, primarily attributed to the persistent elution of NH_4^+ and SiO_4^{4-} hydrolysis of Si_3N_4 particles, leading to the angiogenic and anti-inflammatory properties. NH_4^+ can be assimilated through the glutamine synthetase/glutamate pathway, acting as a nutrient for cells to synthesize proteins, thus promoting cell proliferation and differentiation. On the other hand, SiO_4^{4-} induces angiogenesis and upregulates several antioxidants by modulating gene expression of proangiogenic cytokine receptors and downstream signaling events during silicate bioceramic-induced processes [26]. Moreover, enhanced tensile property of CCS makes it suitable for wound care in areas of the body that undergo regular exercise, such as the knee, ankle, and elbow (Fig. S2).

These unique properties exhibited by Si_3N_4 make it a promising candidate for managing the microenvironment of chronic wounds. To more effectively assess the antibacterial and bioactive properties of CCS, we employed two distinct models for evaluations: an infected wound model and a diabetic wound model, respectively. CCS exhibited promoted comprehensive performance in vivo model including the infected model and diabetic model, indicating that Si_3N_4 could not only effectively eliminate bacteria but also regulate inflammation and promote angiogenesis to facilitate functional wound healing. Nevertheless, further work is still needed to explore the biologic signaling pathways mechanisms of Si_3N_4 in promoting angiogenesis and anti-inflammatory.
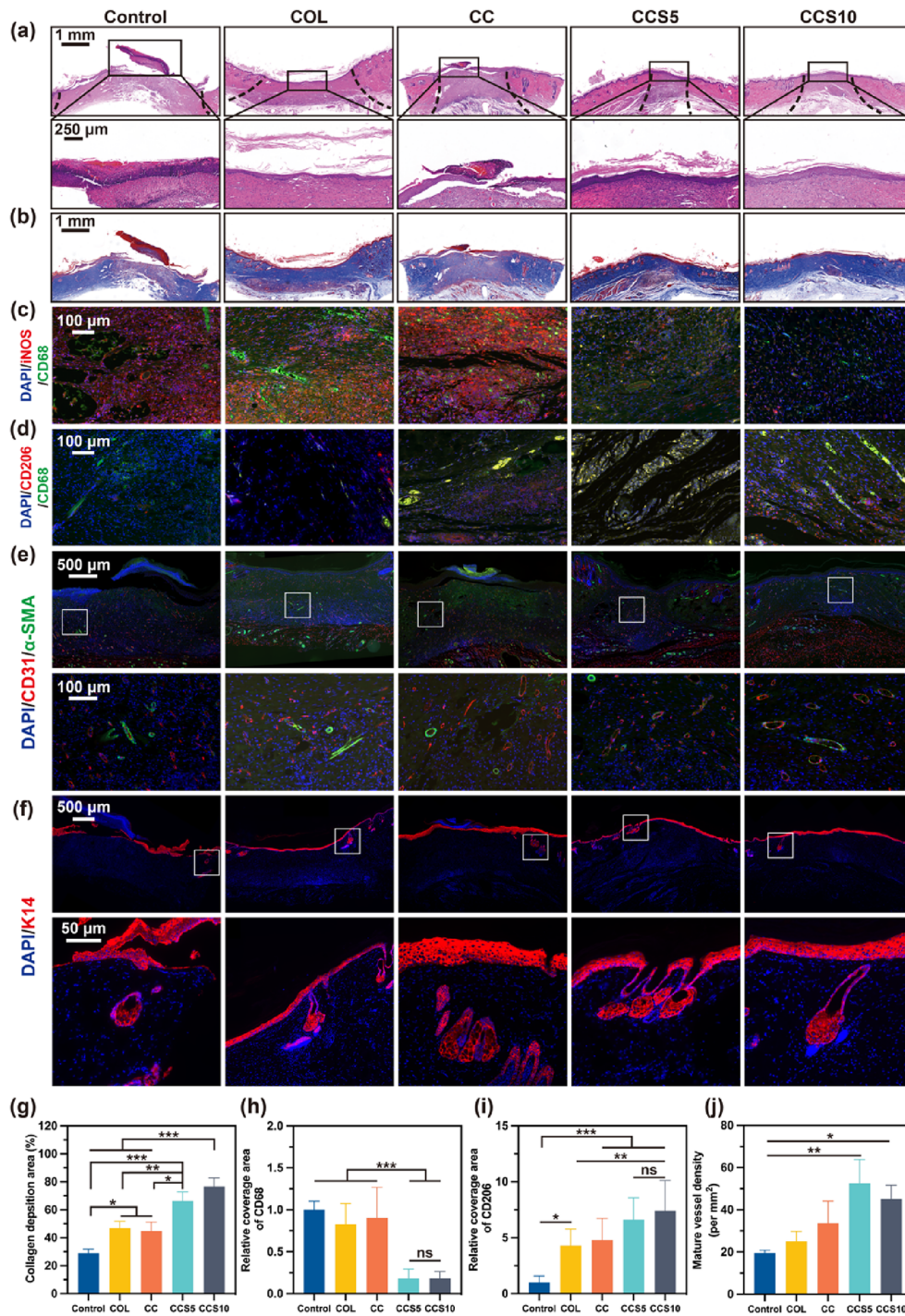
Fig. 7 Effect of CCS on hair follicle remodeling and blood vessel formation in diabetic wounds. **a** H&E staining of the wound tissues with different mats treatments for 4 weeks. The tissue between the black dotted line is unhealed. **b** Masson's trichrome staining, **c** Double immunofluorescence staining of CD68 and iNOS, **d** Double immunofluorescence staining of CD68 and CD206, **e** Double immunofluorescence staining of CD31 and α-SMA, and **f** Immunofluorescence staining of K14 of the wound tissues with different mats treatments for 4 weeks. **g** Collagen deposition area of the wound tissues with different mats treatments for 4 weeks. Relative coverage area of **h** CD68, and **i** CD206. **j** Number of vessels in wound tissues with different mats treatments for 4 weeks

Conclusion

In conclusion, we have developed a novel composite fluffy dressing by the SBS technique, termed CCS, which exhibits superior healing properties for infected and diabetic wounds. The addition of Si_3N_4 particles endows the CCS mat with remarkable antibacterial, angiogenic, and anti-inflammatory capabilities. Notably, the nanofibrous mat containing Si_3N_4 particles exhibited excellent antibacterial activity against bacteria in the early stage of wound healing and refined the microenvironment to significantly accelerate diabetic wound healing by reducing inflammation, promoting collagen deposition and angiogenesis, and forming healthy ECM structure and hair follicles. The findings of this study provide novel insights into the therapeutic role of Si_3N_4 in the healing process of chronic wounds. Taken together, the results highlight the efficiency, safety, and cost-effectiveness of the Si_3N_4-incorporated dressing, offering a promising solution for diabetic wound care.

Supplementary Information The online version contains supplementary material available at https://doi.org/10.1007/s42765-023-00361-w.

Author contributions PM: methodology, investigation, formal analysis, writing—original draft. C-YY: conceptualization, formal analysis, software. CL: data curation, formal analysis. PH: data curation, formal analysis. FY: data curation, investigation. Y-YH: software. JL: writing—review and editing. HW: resources, supervision. QW: resources, supervision. XW: conceptualization, resources, writing—review and editing, supervision, project administration.

Data availability The data that support the findings of this study are available from the corresponding author upon reasonable request.

Declarations

Conflict of Interest All authors certify that they have no affiliations with or involvement in any organization or entity with any financial interest or non-financial interest in the subject matter or materials discussed in this manuscript.

References

1. Bardill JR, Laughter MR, Stager M, Liechty KW, Krebs MD, Zgheib C. Topical gel-based biomaterials for the treatment of diabetic foot ulcers. *Acta Biomater*. **2022**;*138*:73.
2. Las Heras K, Igartua M, Santos-Vizcaino E, Hernandez RM. Chronic wounds: current status, available strategies and emerging therapeutic solutions. *J Control Release*. **2020**;*328*:532.
3. Cao W, Peng S, Yao Y, Xie J, Li S, Tu C, Gao C. A nanofibrous membrane loaded with doxycycline and printed with conductive hydrogel strips promotes diabetic wound healing in vivo. *Acta Biomater*. **2022**;*152*:60.
4. Norahan MH, Pedroza-González SC, Sánchez-Salazar MG, Álvarez MM, de Santiago GT. Structural and biological engineering of 3D hydrogels for wound healing. *Bioactive Mater*. **2023**;*24*:197.
5. Wang C, Liang C, Wang R, Yao X, Guo P, Yuan W, Liu Y, Song Y, Li Z, Xie X. The fabrication of a highly efficient self-healing hydrogel from natural biopolymers loaded with exosomes for the synergistic promotion of severe wound healing. *Biomater Sci*. **2020**;*8*:313.
6. Xu Q, Guo L, Sigen A, Gao Y, Zhou D, Greiser U, Creagh-Flynn J, Zhang H, Dong Y, Cutlar L. Injectable hyperbranched poly (β-amino ester) hydrogels with on-demand degradation profiles to match wound healing processes. *Chem Sci*. **2018**;*9*:2179.
7. Xu Q, Sigen A, Gao Y, Guo L, Creagh-Flynn J, Zhou D, Greiser U, Dong Y, Wang F, Tai H. A hybrid injectable hydrogel from hyperbranched PEG macromer as a stem cell delivery and retention platform for diabetic wound healing. *Acta Biomater*. **2018**;*75*:63.
8. Jung SH, Jang BH, Kwon S, Park SJ, Park TE, Kang JH. Nematic fibrin fibers enabling vascularized thrombus implants facilitate scarless cutaneous wound healing. *Adv Mater*. **2023**. https://doi.org/10.1002/adma.202211149.
9. Edwards R, Harding KG. Bacteria and wound healing. *Curr Opin Infect Dis*. **2004**;*17*:91.
10. Santema TB, Poyck PP, Ubbink DT. Skin grafting and tissue replacement for treating foot ulcers in people with diabetes. *Cochrane Database Syst Rev*. **2016**. https://doi.org/10.1002/14651858.CD011255.pub2.
11. Rowan MP, Cancio LC, Elster EA, Burmeister DM, Rose LF, Natesan S, Chan RK, Christy RJ, Chung KK. Burn wound healing and treatment: review and advancements. *Crit Care*. **2015**;*19*:1.
12. Yang C, Liu G, Chen J, Zeng B, Shen T, Qiu D, Huang C, Li L, Chen D, Chen J, Mu Z, Deng H, Cai X. Chitosan and polyhexamethylene guanidine dual-functionalized cotton gauze as a versatile bandage for the management of chronic wounds. *Carbohyd Polym*. **2022**;*282*: 119130.
13. Liu G, Zhou Y, Xu Z, Bao Z, Zheng L, Wu J. Janus hydrogel with dual antibacterial and angiogenesis functions for enhanced diabetic wound healing. *Chin Chem Lett*. **2023**;*34*: 107705.
14. Liang Y, Li M, Yang Y, Qiao L, Xu H, Guo B. pH/glucose dual responsive metformin release hydrogel dressings with adhesion and self-healing via dual-dynamic bonding for athletic diabetic foot wound healing. *ACS Nano*. **2022**;*16*:3194.
15. Zhou L, Zeng Z, Liu S-Y, Min T, Zhang W, Bian X, Du H, Zhang P, Wen Y. Multifunctional DNA hydrogel enhances stemness of adipose-derived stem cells to activate immune pathways for guidance burn wound regeneration. *Adv Funct Mater*. **2022**. https://doi.org/10.1002/adfm.202207466.

16. Castrejón-Comas V, Alemán C, Pérez-Madrigal MM. Multifunctional conductive hyaluronic acid hydrogels for wound care and skin regeneration. *Biomaterials Science*. **2023**;*11*:2266.

17. Huang J, Zheng Y, Niu H, Huang J, Zhang X, Chen J, Ma B, Wu C, Cao Y, Zhu Y. A multifunctional hydrogel for simultaneous visible H_2O_2 monitoring and accelerating diabetic wound healing. *Adv Healthc Mater*. **2023**. https://doi.org/10.1002/adhm.202302328.

18. Guan Y, Niu H, Wen J, Dang Y, Zayed M, Guan J. Rescuing cardiac cells and improving cardiac function by targeted delivery of oxygen-releasing nanoparticles after or even before acute myocardial infarction. *ACS Nano*. **2022**;*16*:19551.

19. Yang Y, Du Y, Zhang J, Zhang H, Guo B. Structural and functional design of electrospun nanofibers for hemostasis and wound healing. *Adv Fiber Mater*. **2022**;*4*:1027.

20. Xu X-L, Zhou G-Q, Li X-J, Zhuang X-P, Wang W, Cai Z-J, Li M-Q, Li H-J. Solution blowing of chitosan/PLA/PEG hydrogel nanofibers for wound dressing. *Fibers Polym*. **2016**;*17*:205.

21. Pezzotti G, Marin E, Adachi T, Rondinella A, Boschetto F, Zhu W, Sugano N, Bock RM, McEntire B, Bal SB. Bioactive silicon nitride: a new therapeutic material for osteoarthropathy. *Sci Rep*. **2017**;*7*:1.

22. Pezzotti G, Boschetto F, Ohgitani E, Fujita Y, Shin-Ya M, Adachi T, Yamamoto T, Kanamura N, Marin E, Zhu W. Mechanisms of instantaneous inactivation of SARS-CoV-2 by silicon nitride bioceramic. *Mater Today Bio*. **2021**;*12*: 100144.

23. Pezzotti G. Silicon nitride: a bioceramic with a gift. *ACS Appl Mater Interfaces*. **2019**;*11*:26619.

24. Reffitt D, Ogston N, Jugdaohsingh R, Cheung H, Evans BAJ, Thompson R, Powell J, Hampson G. Orthosilicic acid stimulates collagen type 1 synthesis and osteoblastic differentiation in human osteoblast-like cells in vitro. *Bone*. **2003**;*32*:127.

25. Hasilik A, Neufeld E. Biosynthesis of lysosomal enzymes in fibroblasts. Synthesis as precursors of higher molecular weight. *J Biol Chem*. **1980**;*255*:4937.

26. Saghiri MA, Asatourian A, Orangi J, Sorenson CM, Sheibani N. Functional role of inorganic trace elements in angiogenesis—part II: Cr, Si, Zn, Cu, and S. *Crit Rev Oncol Hematol*. **2015**;*96*:143.

27. Kim Y-H, Khan AL, Waqas M, Lee I-J. Silicon regulates antioxidant activities of crop plants under abiotic-induced oxidative stress: a review. *Front Plant Sci*. **2017**;*8*:510.

28. Chattopadhyay S, Raines RT. Collagen-based biomaterials for wound healing. *Biopolymers*. **2014**;*101*:821.

29. Zheng J, Yang C-Y, Wang X. Blow-spun collagen nanofibrous spongy membrane: preparation and characterization. *Tissue Eng C Methods*. **2022**;*28*:3.

30. Wang W, Meng Q, Li Q, Liu J, Zhou M, Jin Z, Zhao K. Chitosan derivatives and their application in biomedicine. *Int J Mol Sci*. **2020**;*21*:487.

31. Rao SB, Sharma CP. Use of chitosan as a biomaterial: studies on its safety and hemostatic potential. *J Biomed Mater Res Off J Soc Biomater Jpn Soc Biomater*. **1997**;*34*:21.

32. Vishu Kumar AB, Varadaraj MC, Gowda LR, Tharanathan RN. Characterization of chito-oligosaccharides prepared by chitosanolysis with the aid of papain and Pronase, and their bactericidal action against *Bacillus cereus* and *Escherichia coli*. *Biochem J*. **2005**;*391*:167.

33. Kravanja G, Primožič M, Knez Ž, Leitgeb M. Chitosan-based (Nano) materials for novel biomedical applications. *Molecules*. **1960**;*2019*:24.

34. Song J, Li Z, Wu H. Blowspinning: a new choice for nanofibers. *ACS Appl Mater Interfaces*. **2020**;*12*:33447.

35. Wang S, Yan F, Ren P, Li Y, Wu Q, Fang X, Chen F, Wang C. Incorporation of metal-organic frameworks into electrospun chitosan/poly (vinyl alcohol) nanofibrous membrane with enhanced antibacterial activity for wound dressing application. *Int J Biol Macromol*. **2020**;*158*:9.

36. Ye W, Yang Z, Cao F, Li H, Zhao T, Zhang H, Zhang Z, Yang S, Zhu J, Liu Z. Articular cartilage reconstruction with TGF-β1-simulating self-assembling peptide hydrogel-based composite scaffold. *Acta Biomater*. **2022**;*146*:94.

37. Ouyang J, Ji X, Zhang X, Feng C, Tang Z, Kong N, Xie A, Wang J, Sui X, Deng L, Liu Y, Kim JS, Cao Y, Tao W. In situ sprayed NIR-responsive, analgesic black phosphorus-based gel for diabetic ulcer treatment. *Proc Natl Acad Sci USA*. **2020**;*117*:28667.

38. Lee Y-C, Chiang C-C, Huang P-Y, Chung C-Y, Huang TD, Wang C-C, Chen C-L, Chang R-S, Liao C-H, Reisz RR. Evidence of preserved collagen in an Early Jurassic sauropodomorph dinosaur revealed by synchrotron FTIR microspectroscopy. *Nat Commun*. **2017**. https://doi.org/10.1038/ncomms14220.

39. Gover Antoniraj M, Angelin Tisha S, Ayyavu M, Shanmugarathinam A, Kandasamy R. Synthesis and characterization of cystamine conjugated chitosan-SS-mPEG based 5-Fluorouracil loaded polymeric nanoparticles for redox responsive drug release. *Eur J Pharm Sci*. **2018**;*116*:37.

40. Xu R, Luo G, Xia H, He W, Zhao J, Liu B, Tan J, Zhou J, Liu D, Wang Y, Yao Z, Zhan R, Yang S, Wu J. Novel bilayer wound dressing composed of silicone rubber with particular micropores enhanced wound re-epithelialization and contraction. *Biomaterials*. **2015**;*40*:1.

41. Wu P, Nelson EA, Reid WH, Ruckley CV, Gaylor JDS. Water vapour transmission rates in burns and chronic leg ulcers: Influence of wound dressings and comparison with in vitro evaluation. *Biomaterials*. **1996**;*17*:1373.

42. Laarz E, Zhmud BV, Bergstrom L. Dissolution and deagglomeration of silicon nitride in aqueous medium. *J Am Ceram Soc*. **2000**;*83*:2394.

43. Dante RC, Kajdas CK. A review and a fundamental theory of silicon nitride tribochemistry. *Wear*. **2012**;*288*:27.

Pengchao Ma is a Ph.D. student in the School of Materials Science and Engineering at Tsinghua University, under the supervision of Dr. Xiumei Wang. His research interests primarily focus on the fabrication and development of tissue engineering and regenerative medicine.

Chun-Yi Yang is currently a PhD student in the School of Materials Science and Engineering at the Tsinghua University under the supervision of Prof. Xiumei Wang. His research centers on the application of nanomaterials, such as nanofibers and nanozymes, in areas such as neural tissue engineering regeneration, wound healing, and rapid hemostasis.

Chengli Li received his Ph.D. degree from Tsinghua University in 2023 and currently works in the Orthopedics Department at Tsinghua Changguang Hospital. His research primarily focuses on the surface modification of biomaterials to enhance bone integration and antibacterial properties.

Peilun Hu graduated from Capital Medical University and now is a Ph.D. Student at the School of Clinical Medicine, Tsinghua University. His research focuses on the construction of multifunctional biomaterials for peripheral nerve regeneration.

Fang Yang received her Ph.D. degree from School of Life Sciences at Tsinghua University in 2023. She has been engaged in research in the fields of microbial engineering, synthetic biology, tissue engineering, and regenerative medicine.

Jiaju Lu received his Ph.D. degree from Tsinghua University in 2019 and now works as an associate professor at the School of Materials Science and Engineering, Zhejiang Sci-tech University. His research mainly focuses on design, synthesis, and application of stimuli-responsive materials for tissue engineering.

Yin-Yuan Huang completed his undergraduate studies at Tsinghua University in Beijing in 2022 and is currently a Ph.D. candidate at Washington University in St. Louis, United States. His research is primarily concentrated on the development and application of plasmonic biosensors.

Hui Wu obtained his Ph.D. in Engineering from Tsinghua University in 2009. He joined the College of Material Engineering, Tsinghua University in 2013, serving as an associate professor. His research focuses on energy storage materials, synthesis and assembly of one-dimensional nanostructured inorganic functional materials, and their structural–functional integration.

Qiong Wu obtained his Ph.D. in Biochemistry and Molecular Biology from Tsinghua University in 2001 and continued to work as a faculty member at the university. He has been engaged in research in the fields of microbial engineering, synthetic biology, tissue engineering, and regenerative medicine.

Yongwei Pan obtained his Ph.D. degree from the School of Medicine, Peking University in 2004. He currently holds a position at the Department of Orthopedics at Changgung Hospital, Tsinghua University since 2016. His primary research areas encompass the investigation of the pathogenesis of brachial plexus neuritis as well as the exploration of orthopedic surgical robots.

Xiumei Wang obtained her Ph.D. degree in Materials Physics and Chemistry from Tsinghua University in 2005. Since 2013, she has been working as a researcher at the College of Material Science, Tsinghua University. Her research primarily focuses on fundamental studies in biomaterials and the development of biomedical materials for clinical applications. This includes the development and clinical translation of regenerative repair materials for tissues such as bone and nerves.